Design Methodology of Feedback-LNAs for GHz Applications

Antonio Liscidini[1], Massimo Brandolini[1], Paolo Rossi[1], Felice Torrisi[2], and Francesco Svelto[1]

(1) Laboratorio di Microelettronica, Università di Pavia, Via Ferrata 1, 27100, Pavia, ITALY
Tel.: (+39) 0382-505227, Fax: (+39) 0382-422583, e-mail: antonio.liscidini@unipv.it
(2) STMicroelectronics, Str. Primosole 50, 95100, Catania, ITALY

ABSTRACT - The design strategy leading to common-base, high linearity feedback-LNAs is proposed. A narrow-band frequency tunable solution and a broad-band one have been designed. Two zero-IF front-ends realized for IEEE 802.11a, HiperLAN2, and HiSWANa including variable-gain mixers, show: 2.5dB NF, -9.5dBm IIP3, and 3.4dB NF, -6dBm IIP3 respectively.

I. INTRODUCTION

Wireless mobile communications handsets ask for highly integrated, low-power, high-performance RF circuit solutions. Telecommunication systems are usually narrow-band, meaning the signal band over carrier ratio is usually small and narrow-band RF circuits, able to process the signal while filtering interferers, are adopted. The evolution towards multi-band multistandard transceivers poses new challenges because the processing circuits are required to operate in a broad band though still being low-noise and linear enough to tolerate inter-modulation distortion from unwanted interferers. In this paper, we focus the attention on low-noise amplifiers for multistandard applications.

The inductively degenerated common-emitter stage allows minimum noise in impedance matching conditions, in narrow-band systems, but does not lend itself to multi-band operation. Considering the continuous rise of device f_T in modern scaled technologies, we exploit the use of feedback, even in the GHz range, to achieve low-noise, high linearity in a broad band under impedance matching condition.

In a way very similar to the well-known design strategy that, starting from the common-emitter amplifier, allows to design the inductively degenerated stage for minimum noise [1], in this paper we arrive at the voltage-voltage feedback-LNA design from the common-base stage. First, for the minimum-size transistor, in the common-base configuration, the optimum current density ($J_{c,opt}$) that corresponds to the minimum achievable noise figure (NF_{opt}) is found. Then, the device is sized in order to satisfy the noise matching condition with a 50Ω source. Finally, the applied voltage-voltage feedback allows to simultaneously achieve impedance matching and voltage gain.

Two different feedback-LNAs, embedded in two receiver front-ends designed for 5-6GHz multistandard wireless LAN applications have been fabricated in a 0.25μm SiGe BiCMOS technology. The first prototype consists of an LNA covering more than 1GHz band, by means of 8 tuneable LC narrow-bands, followed by quadrature mixers. Measured results, reported in [2], are 2.5dB NF, -9.5dBm IIP3 with a current consumption of 16mA from a 2.5V supply. The second prototype differs for the LNA, which is broad-band. The broad input matching and gain profiles are obtained by lowering the quality factor (Q) of the load. This front-end achieves 3.4dB NF, -6dBm IIP3 and consumes 25mA. The two front-ends are designed for zero-IF receive architecture.

II. DESIGN STRATEGY FOR MINIMUM NOISE FIGURE

The design process that leads to the feedback-LNA starts from the minimum-size transistor in common-base configuration. In the first design step the optimum current density $J_{c,opt}$ that corresponds to the device minimum achievable noise figure NF_{opt} is found. NF_{opt} represents the absolute minimum of NF_{min}, which is the NF lower limit, when the common-base device is matched to its optimum noise source, for a given collector current density J_c. An analytical expression for the noise factor F_{min} can be calculated for the common-base stage by using the method proposed in [3] applied to the noise equivalent circuit depicted in figure 1(a).

The base resistance ($r_{bb'}$) thermal noise and the base and collector current shot noise are taken into account, giving:

$$F_{min}=1+\frac{1}{\beta}+\sqrt{2g_m r_{bb'}\left(\frac{\omega^2}{\omega_T^2}+\frac{1}{\beta}\right)+\frac{1}{\beta}} \qquad (1)$$

β is the DC current gain, g_m the device transconductance, ω_T the unity gain frequency.

The same analysis, applied to the common-emitter stage, based on the noise equivalent circuit depicted in figure 1(b), leads to:

$$F_{min}=1+\frac{1}{\beta\left[1+\left(\omega/\omega_T\right)^2\right]}+\sqrt{\frac{2g_m r_{bb'}\left(\frac{\omega^2}{\omega_T^2}+\frac{1}{\beta}\right)+\frac{1}{\beta}}{1+\left(\omega/\omega_T\right)^2}} \qquad (2)$$

0-7803-8618-3/04/$20.00 ©2004 IEEE

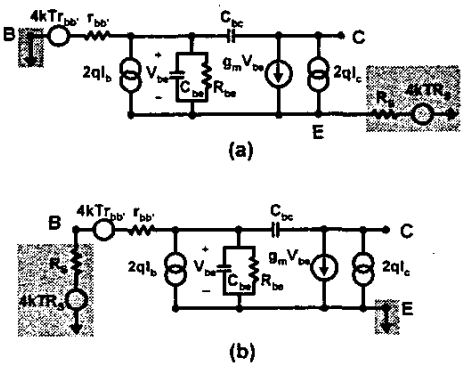

Figure 1. Noise equivalent circuit for common-base (a) and common-emitter (b) amplifiers

where $\omega_T = g_m/C_{bc}$ corresponds to a zero introduced by the parasitic capacitance C_{bc}.

While the effect of C_{bc} is negligible for the common-base topology, it has impact on the common-emitter NF_{min} performance. Equations (1) and (2) have been plotted in figure 2 (continuous lines) and compared with simulation data (dotted lines) at 1GHz and 5GHz.

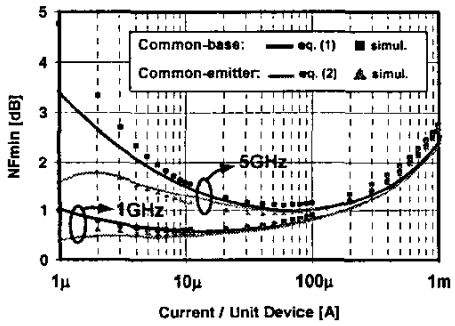

Figure 2. Minimum noise figure (NF_{min}) versus device current density

The agreement between the two is good. From figure 2 it is evident that, when compared to the minimum-size transistor in common-emitter configuration, the common-base amplifier shows the same NF optimum point performance at every frequency. More exactly, the NF_{opt} value for the two amplifier configurations are the same at low frequency, while the common-base topology performs slightly worse at high frequencies, the NF_{opt} difference being 0.1dB at 5GHz. Notice that also the optimum collector current value $J_{c,opt}$ is almost the same for the two amplifier topologies, at the given frequency. The different behavior of the NF_{min} curves for current values far from $J_{c,opt}$ is due to the effect of the base-collector capacitance C_{bc}, not affecting the noise performance of the common-base stage. However, since in the optimum design the active device is biased at the current density $J_{c,opt}$, almost the same noise figure performance will be achieved in either topologies.

Once the optimum collector current $J_{c,opt}$ is found, the noise matching condition has to be satisfied. In fact, for the unit device working at NF_{opt} the optimum noise source $R_{s,opt}$ is different from 50Ω. Since $R_{s,opt}$ is inversely proportional to the device area [1], the transistor emitter stripe length and the number of parallel devices must be increased until $R_{s,opt}$ reaches 50Ω while maintaining the current density at its optimum value. The biasing current is thus increased, and the device works at its NF_{opt} point.

The design steps described so far are the same for both the common-emitter and common-base topologies. Of course, the optimum current and the final device size will be slightly different. The final design step is required to achieve the input impedance matching to the 50Ω source. In the common-emitter configuration, the 50Ω real input impedance is synthesized by means of inductive degeneration. In the common-base configuration the input impedance matching can be achieved by means of a voltage-voltage feedback built around the amplifier [2], as shown in figure 3.

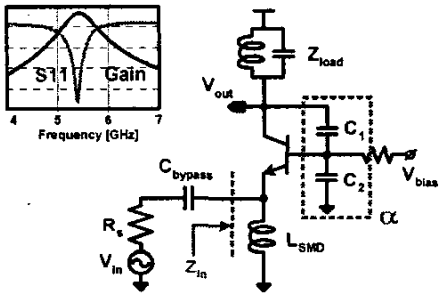

Figure 3. Feedback-LNA diagram of principle

The output impedance is input-reflected and a proper selection of the feedback factor α allows 50Ω-matching.

The design procedure described above leads to the following conclusion: transistor NF_{opt} in the inductively degenerated and common-emitter stages are the same, and so are in the voltage-voltage feedback and common-base stages, since the networks that synthesize the input impedance are made of theoretically noiseless elements. We, therefore, expect the same noise performance from the two topologies.

The use of feedback linearizes the input-output relation, a feature particularly attractive in wireless communications. We will not propose a systematic comparison of different topologies to arrive at expressions of IIP3, because this is rather lengthy. To give insight, let us consider the effect of feedback on the base-emitter voltage signal (v_{be}). By inspection of the circuit:

$$v_{be} = \frac{v_{in}}{2g_m R_S} \quad (3)$$

where v_{in} is the input voltage. Thus the linearity is improved at the expense of current consumption. This conclusion is not as trivial as might appear at a first glance, if we consider, for example, that in a common-base stage the current is set and $v_{be}=v_{in}/2$, under matching conditions. Furthermore, it can be shown that the here proposed feedback-LNA is more linear than the inductively degenerated stage, for the same power consumption.

III. MULTISTANDARD LNA DESIGN

Wireless local area networks in 5GHz frequency range are standardized according to IEEE 802.11a in North America, HiperLAN2 in Europe and HiSWANa in Japan respectively. The presence of such a fragmented distribution suggests two strategies to arrive at a multistandard terminal. In the first, the whole frequency range is finely sliced and a frequency tuneable LC load allows to select the different frequency portions in the range, realizing a multi-band amplifier. In the second a wide-band LNA is adopted.

The two solutions differ for the output stage. In fact, assuming L_{SMD} an high impedance at the frequency of interest, the input impedance Z_{in} and the frequency transfer function of the amplifier depicted in figure 3 are given by:

$$Z_{in} = \frac{1}{g_m} + \alpha Z_{load} \quad (4)$$

$$G_V = \frac{Z_{load}}{R_S + \frac{1}{g_m} + \alpha Z_{load}} \quad (5)$$

where α is the feedback factor, Z_{load} and R_S are the load impedance and source resistance, respectively. From equations (4) and (5) the load impedance determines both the input matching and the peak gain frequency. A proper selection of the load impedance allows to arrive either at a multi-band amplifier or at a wide-band one.

The multi-band amplifier covers the whole frequency range by means of a resonant load tunable through a bank of binary weighted capacitors: three switches provide eight different configurations (Figure 4(a)).

In the second approach a resonant load with a lower quality factor is used to broaden the input-matching and the voltage-gain frequency bands. In this wider-band approach only two different modes are required to cover the whole frequency range, simplifying the band selection. The load tuning is realized reducing the value of the inductance in the tank by means of a switch in parallel with the inductor

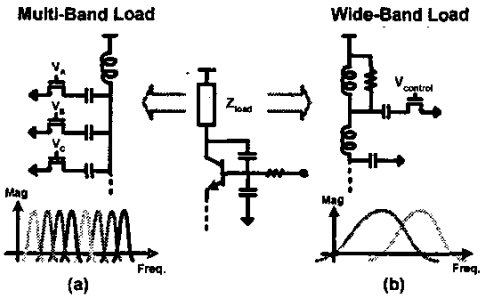

Figure 4. Load implementation for the multi-band (a) and wide-band (b) prototypes

(Figure 4(b)).

The multi-band approach is more complex because three switches are required to control the different bands while in the wide-band approach only one switch is needed. On the other hand, the lower quality factor determines an increase in the overall LNA noise figure. The noise performance of the multi-band LNA is indeed superior.

In the two front-end prototypes the LNAs are followed by quadrature variable-gain down-converters, designed as modified Gilbert cells [2]. These stages make use of pseudo-differential NMOS V-I converters, for maximum IIP3, and bipolar switching pairs, to exploit their superior noise performance, critical in the adopted zero-IF architecture.

IV. EXPERIMENTAL RESULTS

The two prototypes have been fabricated in the 0.25µm SiGe BiCMOS7G process from STMicroelectronics, and housed in 36-pin QFN plastic packages. All the pads are ESD protected. Silicon active area is roughly the same and equal to 0.85mm^2 for the two implementations. Figure 5 provides the two die photomicrographs.

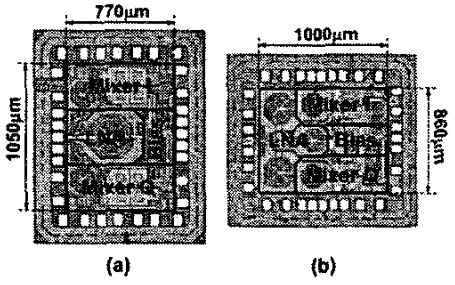

Figure 5. Multi-band (a) and wide-band (b) front-end die photomicrographs

Figure 6 shows the measured gain profile for the multi-band front-end. The curves are obtained changing all the 8 configurations of the switches in the multi-band LNA, keeping the externally provided local oscillator 500kHz away from the input signal.

The IEEE 802.11a, HiperLAN2, and HiSWANa bands are covered with margin and the front-end gain is higher than 31dB in each band of interest.

In the wide-band front-end a 28dB maximum gain is achieved, as shown in figure 7. In each band, the peak-gain frequency is slightly lower than expected, due to parasitics not completely taken into account in the design phase.

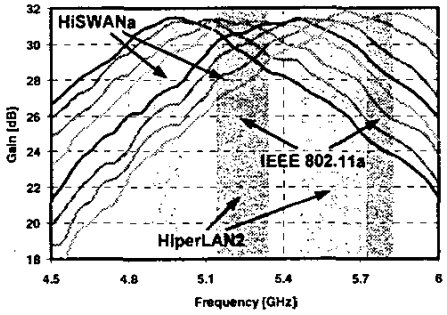

Figure 6. Multi-band front-end gain versus frequency

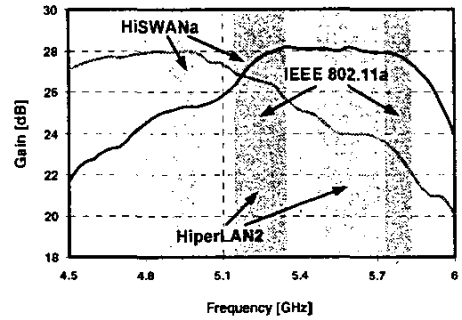

Figure 7. Wide-band front-end gain versus frequency

Noise figure was evaluated by means of an HP346B noise source. External operational amplifiers were used in order to raise the front-end output noise allowing measurements by means of a 50-Ω input HP8564E spectrum analyzer. The front-end that embeds the multi-band LNA features a noise figure as low as 2.5dB in high-gain mode. In low-gain mode, the noise figure becomes 2.9 dB. The front-end with the wide-band LNA shows 3.4dB and 4.1dB noise figure in high and low-gain modes, respectively.

Third-order non-linearity was evaluated injecting tones 20MHz and 40.5MHz away from the LO frequency. Measured results for the prototype embedding the wide-band LNA are -6dBm IIP3 in high-gain mode and -2.5dBm in low-gain mode. The front-end with the multi-band LNA features -9.5dBm and -6dBm in the two gain modes. In fact, the multi-band solution was designed to achieve minimum noise, while the wide-band one has a better linearity by virtue of a lower LNA gain.

Table I summarizes the measured performance. The current consumption is 16mA for the prototype that embeds the narrow-band LNA, while the other one draws 25mA from the 2.5V supply.

	Front-end with narrow-band LNA		*Front-end with wide-band LNA*	
Gain condition	**High**	**Low**	**High**	**Low**
Gain	**31.5dB**	**20.5dB**	**28dB**	**20dB**
NF	**2.5dB**	**2.9dB**	**3.4dB**	**4.1dB**
IIP3	**-9.5dBm**	**-6dBm**	**-6dBm**	**-2.5dBm**
IIP2	**23dBm**	**31dBm**	**26dBm**	**37dBm**
Current	**16mA**		**25mA**	
Supply	**2.5V**			

Table I. Performance summary

V. CONCLUSIONS

The design methodology that, starting from the common-base amplifier, leads to the design of a voltage-voltage feedback-LNA is presented. The proposed strategy is applied to the design of two LNA prototypes embedded in two multistandard zero-IF front-ends tailored to the 5-6GHz wireless LANs. In the first prototype the LNA is designed for very low noise, and the front-end achieves 2.5dB NF, -9.5dBm IIP3 while consuming 16mA from a 2.5V supply. The second prototype, designed for higher linearity, embeds a wide-band LNA, and features 3.4dB NF, -6dBm IIP3 while drawing 25mA.

VI. ACKNOWLEDGEMENTS

This research has been supported by the Italian National Program Firb, contract n°RBNE01F582. The authors thank D. Arrigo, M. Paparo (STMicroelectronics) and R. Castello (Università di Pavia) for fruitful discussions, M. Bonaventura and R. Sciuto (STMicroelectronics) for technology access and circuit layout.

VII. REFERENCES

[1] O. Shana's, I. Lindscott, and L. Tyler, "Frequency-Scalable SiGe Bipolar RF Front-end Design", *IEEE J. of Solid-State Circuits*, vol.36, n.6, pp. 888-895, June 2001.

[2] P. Rossi, A. Liscidini, M. Brandolini, and F. Svelto, "A 2.5dB NF Direct-Conversion Receiver Front-End for HiperLAN2/IEEE802.11a", *in IEEE Solid-State Circuits Conference (ISSCC), Digest of Technical Papers*, vol.1, pp. 102-103, Feb. 2004.

[3] G. Niu, J. D. Cressler, S. Zhang, W. E. Ansley, C. S. Webster, and D. L. Harame, "A Unified Approach to RF and Microwave Noise Parameter Modeling in Bipolar Transistor", *IEEE Trans. on Electron Devices*, vol.48, n.11, pp. 2568-2574, Nov. 2001.